

Observation of quantum strong Mpemba effect

Received: 14 February 2024

Accepted: 7 November 2024

Published online: 06 January 2025



Jie Zhang^{1,2,3,9}, Gang Xia^{1,9}, Chun-Wang Wu^{1,2,3}, Ting Chen^{1,2,3}, Qian Zhang⁴, Yi Xie^{1,2,3}, Wen-Bo Su¹, Wei Wu^{1,2,3}, Cheng-Wei Qiu⁵, Ping-Xing Chen^{1,2,3}, Weibin Li^{6,7}✉, Hui Jing^{1,4,8}✉ & Yan-Li Zhou^{1,2,3}✉

An ancient and counterintuitive phenomenon known as the Mpemba effect (water can cool faster when initially heated up) showcases the critical role of initial conditions in relaxation processes. How to realize and utilize this effect for speeding up relaxation is an important but challenging task in purely quantum system till now. Here, we experimentally study the strong Mpemba effect in a single trapped ion system in which an exponentially accelerated relaxation in time is observed by preparing an optimal quantum initial state with no excitation of the slowest decaying mode. Also, we demonstrate that the condition of realizing such effect coincides with the Liouvillian exceptional point, featuring the coalescence of both the eigenvalues and the eigenmodes of the systems. Our work provides an efficient strategy to engineer the dynamics of open quantum system, and suggests a link unexplored yet between the Mpemba effect and the non-Hermitian physics.

Relaxations or dissipative evolutions from initial states to a stationary state, widely existing in nature, are vital for fundamental studies of nonequilibrium phenomena and practical control of dynamical devices^{1,2}. In quantum realm, rapid relaxations are highly desirable for efficient quantum state preparation and qubit engineering^{3–8}. As a possible strategy to achieve this goal, the Mpemba effect (ME)⁹, well-known in the counterintuitive example that water can cool faster when initially heated up, has attracted growing interests both in classical^{10–17} and quantum systems in recent years^{18–30}. Often, this and related phenomena admits a general explanation^{10–12,31}: the state of the hotter system overlaps less with the slowest decaying mode (SDM) of the dissipative or cooling dynamics, implying the critical role of initial conditions in relaxations (see Fig. 1(a, b)).

For purely quantum systems at zero temperature, the main challenge is to identify ME-induced rapid relaxations that are not smeared out by quantum superposition¹⁸. Very recently, Carollo et al.¹⁸

proposed that strong ME (sME) or exponential speed-up of relaxation can emerge in Markovian open quantum systems by devising an optimal initial state (i.e., sME state) to prohibit excitation of the slowest decaying mode (SDM, see Fig. 1(c)). This prediction of quantum sME, however, has not been experimentally realized till now, hindering its possible applications in e.g., ‘engineered’ relaxation dynamics of the open quantum system¹⁴.

Here, we report the observation of the sME in a truly quantum system, which is a genuine quantum effect and cannot be captured by semi-classical methods. As an essential step towards this target, we construct the sME state via efficient gate operations on a single trapped ion and show that with such special pure state, featuring zero overlap with the SDM, exponential speeding-up of relaxations can be observed (see Fig. 1(d–g)). Also we find that a critical point can appear in our system, separating the regimes with or without exponential acceleration of relaxations, which coincides well with the

¹Institute for Quantum Science and Technology, College of Science, National University of Defense Technology, Changsha, China. ²Hunan Key Laboratory of Mechanism and technology of Quantum Information, Changsha, China. ³Hefei National Laboratory, Hefei, Anhui, China. ⁴Key Laboratory of Low-Dimensional Quantum Structures and Quantum Control of Ministry of Education, Hunan Normal University, Changsha, China. ⁵Department of Electrical and Computer Engineering, National University of Singapore, Singapore, Singapore. ⁶School of Physics and Astronomy, University of Nottingham, Nottingham, United Kingdom. ⁷Centre for the Mathematics and Theoretical Physics of Quantum Non-equilibrium Systems, University of Nottingham, Nottingham, United Kingdom. ⁸College of Science, National University of Defense Technology, Changsha, China. ⁹These authors contributed equally: Jie Zhang, Gang Xia.

✉ e-mail: weibin.li@nottingham.ac.uk; jinghui73@foxmail.com; ylzhou@nudt.edu.cn

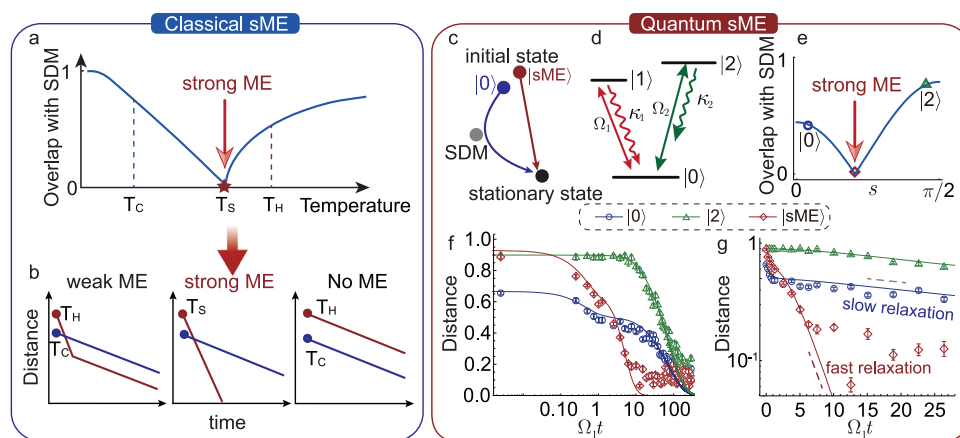


Fig. 1 | Comparison for classic and quantum Mpemba effect. **a** The ME can be understood in an intuitive way: the amplitude of the overlap of the initial state with the slowest decaying mode (SDM) depends on the initial temperature in a non-monotonic way. The SME appears when the overlap with the SDM vanishes. **b** Weak ME: If an initial high temperature state has a smaller SDM amplitude than that of the lower temperature state, it can reach the thermal equilibrium faster. Strong ME: the system reaches equilibrium at an exponentially faster rate. No ME: the initial high temperature state has a larger overlap with the SDM and thus reaches the equilibrium slower. **c** By applying a unitary operation, one can realize an initial SME state and approaches the stationary state with a faster rate. **d** The energy levels for

observing the sME (with $\kappa_2 \ll \kappa_1$). **e** The overlap $|c_1|$ of a rotated initial random state with the SDM as a function of the rotation angle s . **f** The distance between the time-relaxed state $\rho(t)$ and the stationary state ρ_{ss} for different initial states: $|0\rangle$ (blue), $|2\rangle$ (green) and $|sME\rangle$ (red), respectively. The initial SME state starts with a longer distance from ρ_{ss} than the initial state $|0(2)\rangle$ but reaches ρ_{ss} faster. **g** The logarithmic scale of the distance evolves with time for different initial states. An exponential speed-up of relaxation is clearly observed for the SME initial state. The experimental parameters for (e–g) are $\Omega_1 = 2\pi \times 20$ kHz, $\Omega_2 = 0.06\Omega_1$, $\kappa_1 = 2\Omega_1$, $\kappa_2 = 0.0015\Omega_1$, and the solid lines here are the theoretical predictions based on the experimental parameters.

Liouvillian exceptional point (LEP)^{32–39}. Furthermore, we observe both eigenvalues and eigenmodes coalesce at the LEP in the experiment by measuring the overlaps with the decaying modes. Our findings indicate a possible link unexplored yet between quantum ME and non-Hermitian physics^{7,38–44}, which may stimulate more exciting efforts on e.g., engineering quantum SME with higher-order or topological LEPs^{38,39,44}.

Results

Theory of quantum strong Mpemba effect

To understand the quantum SME, we consider a Lindblad master equation $\dot{\rho} = \mathcal{L}\rho(t)$, where \mathcal{L} is the Liouvillian superoperator^{18,36,45}

$$\mathcal{L}\rho = -i[H, \rho] + \sum_{\alpha} \left(J_{\alpha} \rho J_{\alpha}^{\dagger} - \frac{1}{2} \{ J_{\alpha}^{\dagger} J_{\alpha}, \rho \} \right). \quad (1)$$

Here H is the Hamiltonian of the system and J_{α} are the quantum jump operators. The density operator $\rho(t)$ can be expanded as the sum of all eigenmodes (R_i) of \mathcal{L}

$$\rho(t) = e^{\mathcal{L}t} \rho_{ss} + \sum_{i=1}^{d^2-1} c_i e^{\lambda_i t} R_i. \quad (2)$$

Here $R_i(L_i)$ are the right (left) eigenmatrices of the Liouvillian superoperator \mathcal{L} , with the corresponding eigenvalues $\lambda_0 > \text{Re}[\lambda_1] \geq \text{Re}[\lambda_2] \geq \text{Re}[\lambda_3] \geq \dots$, and $\lambda_0 = 0$. λ_0 or its eigenmatrix R_0 denotes the stationary state ρ_{ss} , which is independent of any initial state ρ_{in} , while the real parts of other eigenvalues $\lambda_{i \geq 1}$ indicate the relaxation rates of the eigenmodes R_i . Coefficients $c_i = \text{Tr}[L_i \rho_{in}]$ give the overlap of L_i with ρ_{in} , and d^2 denotes the number of the decay modes.

Generally, an initial state can overlap with all decaying modes of Lindblad dynamics, but at long times the relaxation is dominated by the slowest one R_1 ^{13,15,45,46}. The decay rate of the eigenmode R_1 sets an exponential timescale of the relaxation $\tau_1 = 1/|\text{Re}[\lambda_1]|$ ^{45–47}, which is normally independent of the initial state. But for the ME case, anomalous fast relaxations can be achieved by designing a special form of

the overlap c_1 featuring smaller or even zero overlap with the SDM^{11,13,18,20}.

The quantum SME can be realized by designing such an initial state $|sME\rangle$ satisfying¹⁸,

$$\text{Tr}[L_1 |sME\rangle \langle sME|] = c_1 = 0. \quad (3)$$

This optimal state $|sME\rangle$ is prepared by applying a well devised unitary transformation to an initially pure quantum state of the system¹⁸. Therefore the SME state is normally a quantum superposition state, which represents a fundamental difference from classic SME, and thus the resulting dynamical behaviour cannot be captured by semi-classical approaches (see Supplementary note 1). Since this SME initial state has zero overlap with the SDM, the relaxation rate of the system is thus $|\text{Re}[\lambda_2]|$, with the timescale $\tau_2 = 1/|\text{Re}[\lambda_2]|$, instead of $\tau_1 = 1/|\text{Re}[\lambda_1]|$. This implies an exponentially faster convergence to the stationary state by a factor $\text{Re}[\delta\lambda_{12}] = \text{Re}[\lambda_1 - \lambda_2]$.

Experimental approach

The experimental setup and relevant energy levels for the quantum SME are shown in Fig. 2(a, b). The ground state $|0\rangle = |4^2S_{1/2}, m_j = -1/2\rangle$ is resonantly coupled to state $|1\rangle = |3^2D_{5/2}, m_j = -5/2\rangle$ and $|2\rangle = |3^2D_{5/2}, m_j = 3/2\rangle$ by one 729 nm laser beam with two frequency components and the corresponding Rabi frequencies are Ω_1 and Ω_2 , respectively. Another laser at 854 nm with right circular polarization induces a tunable decay channel between state $|1\rangle$ and $|0\rangle$ with decay rate κ_1 , by coupling $|1\rangle$ to a short-life level $|4^2P_{3/2}, m_j = -3/2\rangle$, which will decay quickly back to the state $|0\rangle = |4^2S_{1/2}, m_j = -1/2\rangle$ (see Supplementary note 2). The imperfect polarization of 854 nm will cause slow decay from state $|2\rangle$ to $|0\rangle$ with decay rate $\kappa_2 \ll \kappa_1$ and also the leakage of population to the other Zeeman ground state. Fortunately, the leakage problem can be fixed by introducing a weak optical pumping beam at 397 nm during the data acquisition process. Then for the effective three-level system, we have the Hamiltonian $H = \sum_{j=1,2} \Omega_j/2(|0\rangle \langle j| + |j\rangle \langle 0|)$ and two jump operators $J_j = \sqrt{\kappa_j}|0\rangle \langle j|$ ($j = 1, 2$).

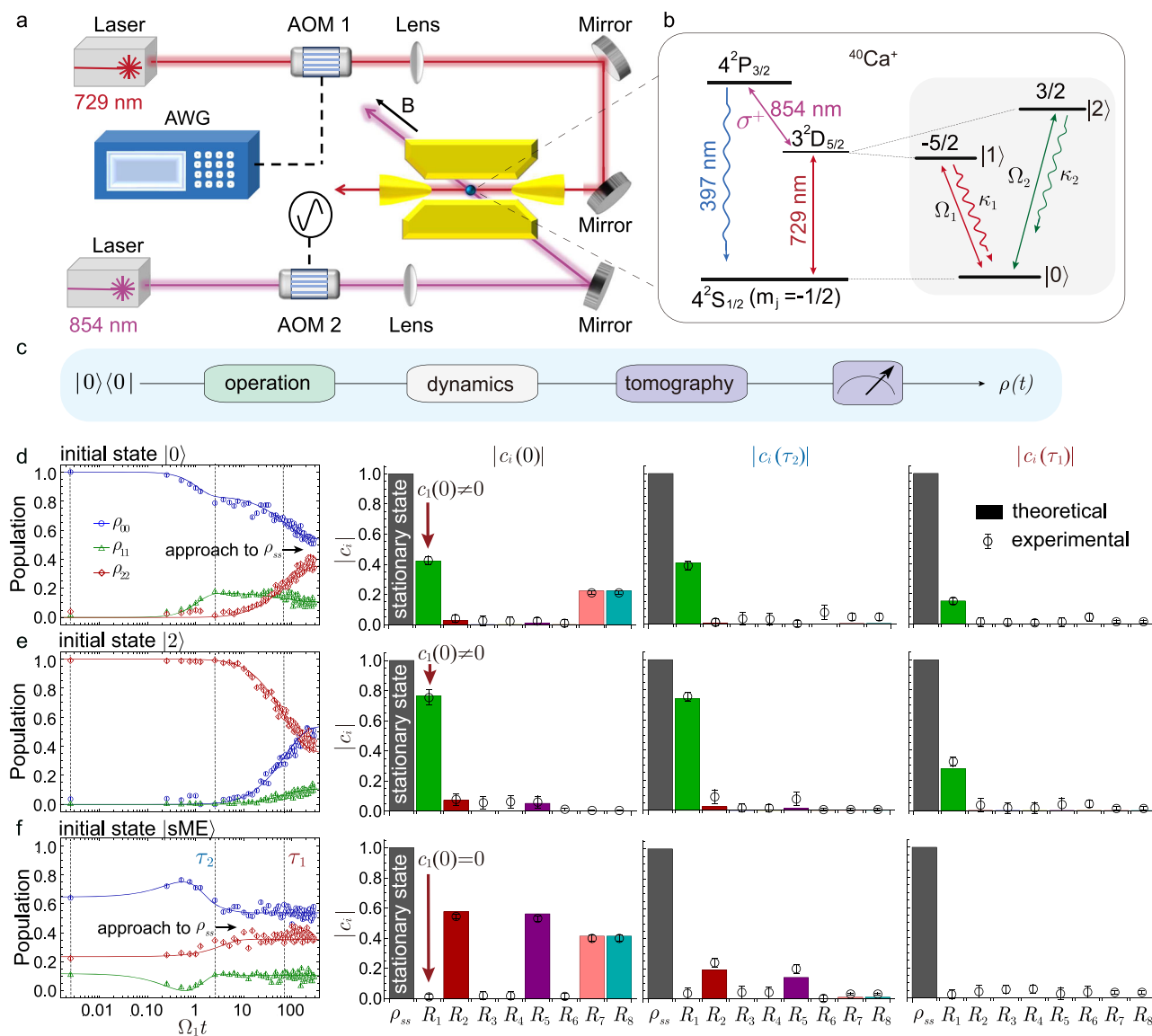


Fig. 2 | Experimental setup and relaxation dynamics for different initial states.

a Experimental setup of quantum SME. The coherent driving between the S state and D state is realized by using a 729 nm laser beam with linewidth about 100 Hz. Two transitions required (as shown in **b**) are simultaneously driven by injecting two RF frequencies to an acoustic-optic modulator (AOM1) via an arbitrary waveform generator (AWG). The decay rate of the D state is controlled by the power of 854 nm laser. **b** The relevant energy levels of a single $^{40}\text{Ca}^+$ ion involved in the experiment, with state $|0\rangle$, $|1\rangle$, $|2\rangle$ are encoded in the energy levels $|4^2S_{1/2}, m_j = -1/2\rangle$, $|3^2D_{5/2}, m_j = -5/2\rangle$ and $|3^2D_{5/2}, m_j = 3/2\rangle$, respectively. The energy gap of state $|1\rangle$ and $|2\rangle$ can minimize detrimental effect from the polarization impurity of the 854

nm laser beam. **c** Protocol to generate the sME initial state and tomography of the density matrix $\rho(t)$. After generating the initially sME state by applying two rotation gates on the state $|0\rangle$, the system evolves with the Liouvillian superoperator \mathcal{L} of interest. After a time t , projective measurements are performed for the tomography of the state $\rho(t)$. **d–f** Left: The dynamics of the state population $\rho_{ii} = \text{Tr}[|i\rangle\langle i|\rho(t)]$ ($i = 0, 1, 2$) for initial states $|0\rangle$ (**d**), $|2\rangle$ (**e**) and $|sME\rangle$ (**f**) on a logarithmic timescale. Right: The evolving overlap $|c_i(t)| = |\text{Tr}[L_i\rho(t)]|$ for three time stamps at 0, τ_2 , τ_1 . The solid lines indicate the theoretical results based on the experimental parameters same with Fig. 1(e–g) and the error bars are generated by using Monte Carlo simulation.

To observe quantum SME, we initialize the ion in the ground state $|0\rangle$ and subsequently rotate it by applying a unitary operation U^{48} (see Fig. 2(c)). Although this transformation can be exactly constructed through the decomposition method⁴⁸, it is still challenging to realize it with high fidelity in the experiment since at least six gate operations are required for our case. To overcome this obstacle, here we optimize the operations to two qubit-rotations (see “Methods” for technical details). The rotated state then relaxes with the desired Liouvillian superoperator \mathcal{L} . The final step is quantum state tomography, i.e., performing the projective measurements on the time-relaxed state $\rho(t)$ as it relaxes from the initial state ρ_{in} to the final stationary ρ_{ss} . We remark that both the dynamical process and the state readout need to

be carefully regulated, accompanying with the optimization procedure (see “Methods”).

Quantum strong ME

With the aid of tomography of $\rho(t)$, we can characterize the relaxation process by using the Hilbert-Schmidt distance¹⁸

$$D(\rho(t), \rho_{ss}) = \|\rho(t) - \rho_{ss}\|, \quad (4)$$

with the notation $\|A\| = \text{Tr}[\sqrt{A^\dagger A}]$. As presented in Fig. 1(f), the sME initial state generated by our method is farther from the stationary state than normal initial states $|0(2)\rangle$. This is due to the fact that while U

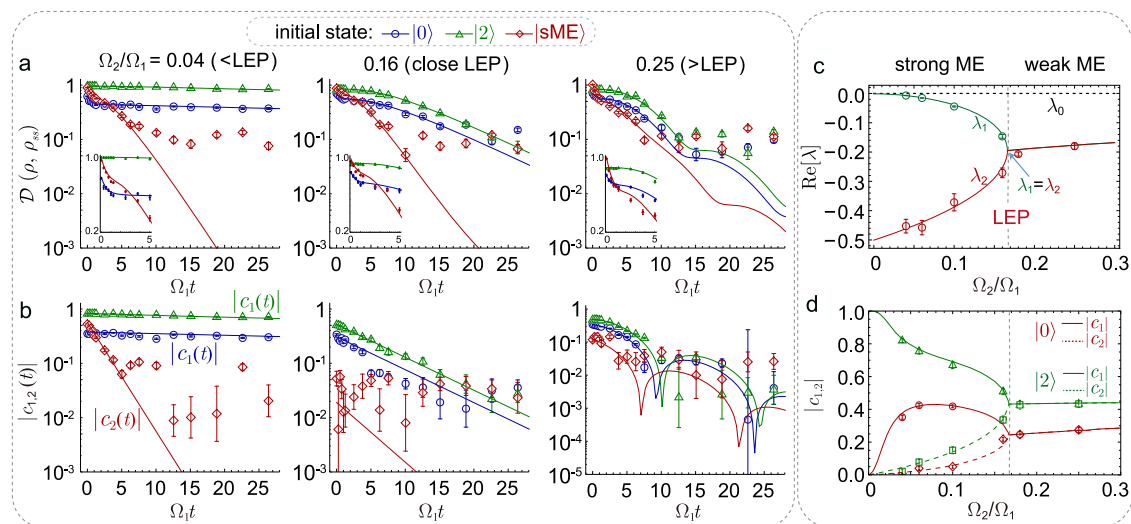


Fig. 3 | From strong ME to weak ME. a Logarithmic scale of distance $\mathcal{D}(\rho, \rho_{ss})$ evolves with time for different initial state: $|0\rangle$ (blue), $|2\rangle$ (green) and $|sME\rangle$ (red), respectively. **b** The corresponding coefficients $c_1(t)$ (of initial state $|0(2)\rangle$) and $c_2(t)$ (of initial state $|sME\rangle$). The sME that exits exponential acceleration is observed for $\Omega_2/\Omega_1 = 0.04, 0.16$ ($< \text{LEP}$). When $\Omega_2/\Omega_1 = 0.25$ ($> \text{LEP}$), $|sME\rangle$ has the same decay rate

with the normal initial states $|0(2)\rangle$, meaning the strong ME disappears but weak ME is allowed. **c** Real parts of the eigenvalues of the Liouvillian operator as a function of Ω_2/Ω_1 . **d** Overlaps $|c_1|$ (solid) and $|c_2|$ (dashed) for different initial states $|0\rangle$ (red) and $|2\rangle$ (green), respectively. The parameters are $\Omega_1 = 2\pi \times 20$ kHz, $\kappa_1 = 2\Omega_1$, $\kappa_2 = 0.0015\Omega_1$. All error bars in this figure are calculated by using Monte Carlo simulation.

removes the SDM excitation, it also modifies the excitation of the remaining ones¹⁸. Nonetheless, the approach to stationarity for sME initial state is still faster since the SDM (R_1) is cut off by U ⁴⁸. Figure 1(g) gives the Logarithmic scale of distance $\mathcal{D}(\rho(t), \rho_{ss})$. Compared with the normal initial states, an exponential speeding-up of the relaxation is reached for the sME initial state, a clear evidence of quantum sME. It can also be observed by other distance measures, for instance, the trace distance⁴⁸ or Bures distance^{49,50} (see Supplementary note 1).

Figure 2(d–f) illustrates the relaxation dynamics of initial states $|0\rangle$, $|2\rangle$, and $|sME\rangle$, respectively, under same experimental parameters. We find that they all reach the same steady state after a sufficiently long time, but the relaxation time of the sME initial state is significantly shorter. For the normal initial states $|0(2)\rangle$ (see Fig. 2(d, e)), when $t \gg \tau_2$ the system relaxes into a state in the metastable manifold till $\tau_1 = 1/|\text{Re}[\lambda_1]|$ ⁴⁵. Differently, as seen in Fig. 2(f), the application of U , cutting of the excitation of the SDM, leads to striking faster approach to the steady state with the time scale $\tau_2 \ll \tau_1$. In order to visualise their overlaps on each decaying mode, we give all coefficients $c_i(t)$ of $\rho(t)$ decomposition into all the decaying modes at time $t = 0$, $t = \tau_2$, and $t = \tau_1$, respectively. As depicted in Fig. 2(d, e), when time $t = 0$, a generic initial state will normally overlap with the slowest one, i.e., $c_1(0) \neq 0$. When time $t > \tau_2$, the overlap of initial state with the short-life excitation modes ($R_{i>1}$) becomes very small, while the SDM (R_1) is still relevant and keeps the system away from stationarity for a long time till $t \gg \tau_1$. However, for the sME initial state, $c_1 = 0$, therefore, the relaxation time scale is reduced to τ_2 with a faster decay rate $|\text{Re}[\lambda_2]|$ (see Fig. 2(f)). Note that the coefficient on R_0 (i.e., the stationary state) has the form $c_0(t) = \text{Tr}[L_0 \rho(t)] = \text{Tr}[\rho(t)] = 1$ and consistently remains at 1 for all the time, while the coefficients on other decay modes $c_i(t) = c_i e^{\lambda_i t} = \text{Tr}[L_i \rho_{in}] e^{\lambda_i t}$ ($i = 1, 2, \dots$) decrease with time for the reason $\text{Re}[\lambda_i] < 0$.

From strong ME to weak ME

Can this exponential acceleration always happen for the sME initial state? To check this, we measure the distance $\mathcal{D}(\rho(t), \rho_{ss})$ and the overlaps $c_{1,2}(t)$ for different parameters of the system. As shown in Fig. 3(a–b), for the normal initial state $|0\rangle(|2\rangle)$, the distance has similar dynamical behavior with the overlap $c_1(t)$ at the final stage of the relaxation, i.e., $\rho(t) - \rho_{ss} \simeq c_1 e^{\lambda_1 t} R_1$. While for sME initial state, it

becomes to $\rho(t) - \rho_{ss} \simeq c_2 e^{\lambda_2 t} R_2$. When $\Omega_2/\Omega_1 \ll 1$, the accelerated relaxation achieved for sME initial state is very significant, since in this regime $|\text{Re}[\lambda_1]| \ll |\text{Re}[\lambda_2]|$, as shown in Fig. 3(c). While as Ω_2 increases, this exponential gain $|\text{Re}[\delta\lambda_{12}]|$ decreases and even disappears when Ω_2 passes across the LEP, where $\lambda_1 = \lambda_2$ and $R_1 = R_2$. The reason is that when $\Omega_2/\Omega_1 > \text{LEP}$, the eigenvalue of the SDM of the \mathcal{L} forms a complex conjugate pair, i.e., $\lambda_1 = \lambda_2^*$ (see Fig. 3(c)), which means that the decaying modes R_1 and R_2 have the same decay rate. Meanwhile, the imaginary parts of eigenvalues $\lambda_{1,2}$ result in the oscillating during the relaxation process^{7,43} (Supplementary note 1). Even though, comparing with normal initial states which have two SDMs, the sME initial state here just has one so that it may still be faster to the stationary state. Different with sME featuring a faster decay rate, this acceleration here corresponds to the weak ME which is associated with a smaller overlap with the SDM¹¹. As a consequence, LEP is the boundary between the quantum strong ME and weak ME, showing that an existence of the quantum strong ME is limited to the regime in which λ_1 is real. It is helpful for deepening the understanding of the relaxation speed limit from both LEPs and quantum ME perspectives.

Based on the measurements of the overlaps, we further demonstrate both eigenvalues (Fig. 3(c)) and eigenmodes (Fig. 3(d)) coalesce at LEP in the experiment. Whereas the impact of the decaying modes is often limited to transient dynamics, it presents a practical challenge for experimental observation of more than one eigenvalue of \mathcal{L} . Normally, LEP happens at the point that an eigenvalue changes from real to complex^{38,39}. However, this change just can show where LEP happens, but does not demonstrate the coalesce of the LEP, because the coalesce of LEPs typically occur in two or more eigenvalues. This challenge could be solved by fitting the measurement of $c_i(t) = c_i e^{\lambda_i t}$ using a single exponential function of time. Based on this, theoretically, one can get the full spectrum of \mathcal{L} . For our system here, considering the overlap c_2 is very small for initial state $|0(2)\rangle$, we choose to get λ_2 by measuring $c_2(t)$ of initial sME state and λ_1 by measuring $c_1(t)$ of initial state $|0\rangle$. The results, as depicted in Fig. 3(c), match well with the theoretical results and show that LEP is signaled by the degenerated of $\lambda_{1,2}$.

As shown in Fig. 3(d), the coalesce of the eigenmodes $R_1(L_1)$ and $R_2(L_2)$ at LEP is indicated by $c_1 = c_2$ for a fixed initial state, because at LEP $\text{Tr}[L_1 \rho_{in}] = \text{Tr}[L_2 \rho_{in}]$. This means the coalesce the coefficients is a detectable way to show the eigenmodes coalesce of LEP. Note that, as we observed in Fig. 3(c–d), the bifurcation singularity of the spectrum

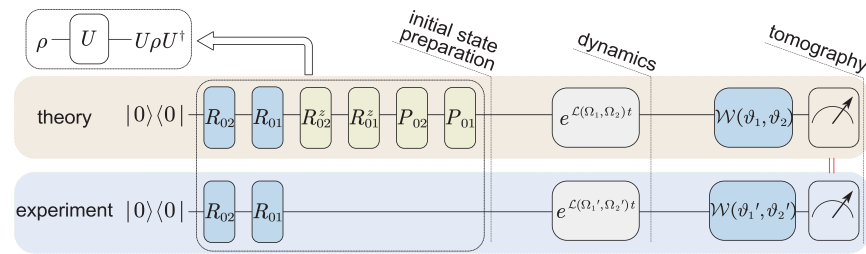


Fig. 4 | Protocol to prepare arbitrary pure qutrit (three-level) states and to get the density matrix $\rho(t)$ in the experiment. First, we construct the quantum state by engineering an 'virtual' but efficient unitary transformation $U = R_{02}R_{01}$. Then in

the dynamical process, the parameters of the lasers $\Omega_{1,2}$ are adjusted accordingly to $\Omega_1 e^{i\phi}$ and $\Omega_2 e^{i\phi'}$. Finally, the state tomography operations are changed accordingly to $\mathcal{W}(\vartheta'_1, \vartheta'_2)$.

and the overlaps $c_{1,2}$ is not detectable in the steady state but rather in the relaxation process³⁶. In fact, for the dynamics at long times, $\rho(t) - \rho_{ss} \simeq c_1 e^{\lambda_1 t} R_1$, thus LEP corresponds the final direction change of the dynamics from R_1 to $R_1 + R_1^\dagger$. This direction change occurring at LEP is the further evidence of a direct link with anomalous phenomena arising in the relaxation process such as sME and the dynamical phase transition^{15,51}.

Discussion

In summary, we have observed the quantum sME in a single trapped-ion system by preparing an optimal pure state that has zero overlap with the SDM. For the quantum sME initial state, we propose an efficient quantum control technique for state preparation, dynamical engineering and state tomography. In addition, we reveal that quantum sME only happens within a certain parameter range, which is determined by LEP. Together with well-developed techniques of engineering quantum states, our work not only provides a powerful tool for exploring and utilizing the quantum sME as examples of engineered relaxation dynamics¹⁴ but also bridges the LEP and quantum ME, two previously independent effects. Besides, the experimentally accessible methods discussed in the present manuscript, such as the efficient unitary transformation and the overlaps measurement, will be valuable tools to assess the quality of the state preparation and the control of the system relaxation.

Note added: While submitting our manuscript, we became aware of another two experimental studies of the Mpemba effect performed with trapped ion systems appeared on arXiv, and currently they have been published on Phys. Rev. Lett^{29,30}.

Methods

We explain here how to devise the unitary transformation U to generate the quantum sME initial (pure) state $\rho_{in}^{sME} = |\text{sME}\rangle\langle\text{sME}|$. We firstly use the method performed in ref. 18 to get $|\text{sME}\rangle$, then we explicitly construct feasible operation U based on our experimental setting (see Fig. 4).

As discussed in ref. 18, the formula of this unitary can be expressed as

$$U = \exp[-is(|\phi_1\rangle\langle\phi_2| + |\phi_2\rangle\langle\phi_1|)]|\phi_1\rangle\langle 0|, \quad (5)$$

where $|\phi_{1(2)}\rangle$ are the eigenstates of the left-hand eigenmatrix L_1 with the corresponding negative (positive) eigenvalues $\alpha_{1(2)}$, $s = \arctan(\sqrt{|\alpha_1/\alpha_2|})$. This qutrit (three-level) U operations can be decomposed into several qubit (two-level) rotations⁴⁸. Compared with qubit operations, a notable challenge in qutrit operations is that the elementary qubit operations lose their 'global-phase' gauge freedom because any phase shift is measured relative to the spectator level⁵².

Now we discuss how to overcome this technical challenge by applying a more efficient and practical way of decomposition, which requires only 2 two-level rotation operations in the experiment (see Fig. 4). Suppose an arbitrary qutrit pure state $|\psi\rangle = U|0\rangle = (a, b, c)^T$ and

$|a|^2 + |b|^2 + |c|^2 = 1$, then U can be decomposed into a product of 2 two-level unitary matrices $U = AB^{48}$, where

$$A = \begin{pmatrix} \frac{a}{\sqrt{|a|^2 + |b|^2}} & \frac{b^*}{\sqrt{|a|^2 + |b|^2}} & 0 \\ \frac{b}{\sqrt{|a|^2 + |b|^2}} & -\frac{a^*}{\sqrt{|a|^2 + |b|^2}} & 0 \\ 0 & 0 & 1 \end{pmatrix}, \quad (6)$$

$$B = \begin{pmatrix} a' & 0 & c^* \\ 0 & 1 & 0 \\ c & 0 & -a^* \end{pmatrix},$$

with $a' = \sqrt{|a|^2 + |b|^2}$. The unitary A and B can be written in the form

$$\begin{aligned} A &= P_{01}(\alpha)Z_{01}(\beta)R_{01}(\gamma, \pi/2)Z_{01}(\delta) \\ &= P_{01}(\alpha)R_{01}^z(\beta + \delta)R_{01}(\gamma, \pi/2 - 2\delta), \\ B &= P_{02}(\alpha')Z_{02}(\beta')R_{02}(\gamma', \pi/2)Z_{02}(\delta') \\ &= P_{02}(\alpha')Z_{02}(\beta' + \delta')R_{02}(\gamma', \pi/2 - 2\delta'), \end{aligned} \quad (7)$$

where

$$P_{01}(x) = \begin{pmatrix} e^{ix} & 0 & 0 \\ 0 & e^{ix} & 0 \\ 0 & 0 & 1 \end{pmatrix}, \quad P_{02}(x) = \begin{pmatrix} e^{ix} & 0 & 0 \\ 0 & 1 & 0 \\ 0 & 0 & e^{ix} \end{pmatrix},$$

$$Z_{01}(x) = \begin{pmatrix} e^{-ix} & 0 & 0 \\ 0 & e^{ix} & 0 \\ 0 & 0 & 1 \end{pmatrix}, \quad Z_{02}(x) = \begin{pmatrix} e^{-ix} & 0 & 0 \\ 0 & 1 & 0 \\ 0 & 0 & e^{ix} \end{pmatrix},$$

$$R_{01}(x, y) = \begin{pmatrix} \cos(\frac{x}{2}) & -ie^{-iy}\sin(\frac{x}{2}) & 0 \\ -ie^{iy}\sin(\frac{x}{2}) & \cos(\frac{x}{2}) & 0 \\ 0 & 0 & 1 \end{pmatrix},$$

$$R_{02}(x, y) = \begin{pmatrix} \cos(\frac{x}{2}) & 0 & -ie^{-iy}\sin(\frac{x}{2}) \\ 0 & 1 & 0 \\ -ie^{iy}\sin(\frac{x}{2}) & 0 & \cos(\frac{x}{2}) \end{pmatrix},$$

and

$$\begin{aligned} \gamma &= 2\arccos|A_{11}|, \\ \alpha &= \frac{1}{2}(\arg(A_{11}) + \arg(A_{22})), \\ \beta &= \frac{1}{2}(\arg(A_{21}) - \arg(A_{11})), \\ \delta &= -\alpha + \arg(A_{22}) - \beta, \\ \gamma' &= 2\arccos|B_{11}|, \\ \alpha' &= \frac{1}{2}(\arg(B_{11}) + \arg(B_{33})), \\ \beta' &= \frac{1}{2}(\arg(B_{31}) - \arg(B_{11})), \\ \delta' &= -\alpha' + \arg(B_{33}) - \beta'. \end{aligned}$$

Here we have translated the phase gates P and Z backwards which implement appropriate phase-shifts between the qutrit states^{52,53}. Then the final decomposed unitary operation for U can be written as

$$\begin{aligned} U &= AB \\ &= P_{01}(\alpha)Z_{01}(\beta + \delta)R_{01}(\gamma, \pi/2 - 2\delta)P_{02}(\alpha') \\ &\quad Z_{02}(\beta' + \delta')R_{02}(\gamma', \pi/2 - 2\delta') \\ &= P_{01}(\alpha)P_{02}(\alpha')Z_{01}(\beta + \delta)Z_{02}(\beta' + \delta') \\ &\quad R_{01}(\gamma, \phi)R_{02}(\gamma', \phi'), \end{aligned} \quad (8)$$

with $\phi = \alpha' - (\beta' + \delta') + \frac{\pi}{2} - 2\delta$, $\phi' = \frac{\pi}{2} - 2\delta'$.

We can further simplify the unitary operation U in a more efficient way by translating phase gates P and Z to the operation backwards till the detection due to the fact that the detection does not need phase information⁵³. By calculating the translated phase in software, we just need two rotation operations $R_{01}R_{02}$ to generate arbitrary qutrit pure state experimentally, which can not only greatly simplify operations, but also improve the fidelity of sME state.

As shown in Fig. 4, our careful analysis shows that the corresponding dynamical operator and state tomography operations need to be modulated accordingly,

$$\mathcal{L}(\Omega_1, \Omega_2) \rightarrow \mathcal{L}(\Omega_1 e^{i\phi}, \Omega_2 e^{i\phi'}). \quad (9)$$

The state tomography for the qutrit system here requires 9 measurement basis, which are $|0\rangle$, $|1\rangle$, $|2\rangle$, $(|0\rangle + |1\rangle)/\sqrt{2}$, $(|0\rangle + i|1\rangle)/\sqrt{2}$, $(|0\rangle + |2\rangle)/\sqrt{2}$, $(|0\rangle + i|2\rangle)/\sqrt{2}$, $(|1\rangle + |2\rangle)/\sqrt{2}$, $(|1\rangle + i|2\rangle)/\sqrt{2}$. However, only S or D state can be detected in the trapped ion system, therefore we need to rotate the basis to state $|0\rangle$ before applying the detection beam since we have encoded state $|1\rangle$ and $|2\rangle$ in D state manifold. The rotation operation $\mathcal{W}(\vartheta_1 e^{i\phi_{11}}, \vartheta_2 e^{i\phi_{12}})$ in the state tomography can be realized by simply combining the π or $\pi/2$ pulses with translating phase $\phi_{11} = \alpha' - 2(\beta + \delta) - (\beta' + \delta')$ on the transition $|0\rangle \leftrightarrow |1\rangle$ and $\phi_{12} = \alpha - 2(\beta' + \delta') - (\beta + \delta)$ on the transition $|0\rangle \leftrightarrow |2\rangle$ respectively. After we get the projective measurement results of these basis, we can reconstruct density matrix by using maximum-likelihood method, and the error bars for the density matrix are obtained by using numerical simulations^{54,55}.

Data availability

The data that supports the findings are presented in the article and Supplementary Information. Source data are provided with this paper.

Code availability

The code used for data analysis and simulation is available from the corresponding author upon request. Source data are provided with this paper.

References

- Breuer, H.-P. & Petruccione, F. *The Theory Of Open Quantum Systems*. (Oxford University Press, 2007).
- Mohseni, M. et al. *Quantum Effects In Biology*. (Cambridge University Press, 2014).
- Verstraete, F., Wolf, M. M. & Cirac, J. I. Quantum computation and quantum-state engineering driven by dissipation. *Nat. Phys.* **5**, 633 (2009).
- Harrington, P. M., Mueller, E. J. & Murch, K. W. Engineered dissipation for quantum information science. *Nat. Rev. Phys.* **4**, 660 (2022).
- Dann, R., Tobalina, A. & Kosloff, R. Shortcut to equilibration of an open quantum system. *Phys. Rev. Lett.* **122**, 250402 (2019).
- Wu, S. L., Ma, W., Huang, X. L. & Yi, X. Shortcuts to adiabaticity for open quantum systems and a mixed-state inverse engineering scheme. *Phys. Rev. Appl.* **16**, 044028 (2021).
- Khandelwal, S., Brunner, N. & Haack, G. Signatures of liouvillian exceptional points in a quantum thermal machine. *PRX Quantum* **2**, 040346 (2021).
- Kumar, P., Snizhko, K., Gefen, Y. & Rosenow, B. Optimized steering: quantum state engineering and exceptional points. *Phys. Rev. A* **105**, L010203 (2022).
- Mpemba, E. B. & Osborne, D. G. Cool? *Phys. Educ.* **4**, 172 (1969).
- Lu, Z. & Raz, O. Nonequilibrium thermodynamics of the Markovian Mpemba effect and its inverse. *Proc. Natl Acad. Sci. USA* **114**, 5083 (2017).
- Klich, I., Raz, O., Hirschberg, O. & Vucelja, M. Mpemba index and anomalous relaxation. *Phys. Rev. X* **9**, 021060 (2019).
- Gal, A. & Raz, O. Precooling strategy allows exponentially faster heating. *Phys. Rev. Lett.* **124**, 060602 (2020).
- Kumar, A. & Bechhoefer, J. Exponentially faster cooling in a colloidal system. *Nature* **584**, 64 (2020).
- Bechhoefer, J., Kumar, A. & Chétrite, R. A fresh understanding of the mpemba effect. *Nat. Rev. Phys.* **3**, 534 (2021).
- Teza, G., Yaacoby, R. & Raz, O. Eigenvalue crossing as a phase transition in relaxation dynamics. *Phys. Rev. Lett.* **130**, 207103 (2023).
- Pemartin, I. G.-A., Mompó, E., Lasanta, A., Martín-Mayor, V. & Salas, J. Shortcuts of freely relaxing systems using equilibrium physical observables. *Phys. Rev. Lett.* **132**, 117102 (2024).
- Ibáñez, M., Dieball, C., Lasanta, A., Godec, A. & Rica, R. A. Heating and cooling are fundamentally asymmetric and evolve along distinct pathways. *Nat. Phys.* **20**, 135–141 (2024).
- Carollo, F., Lasanta, A. & Lesanovsky, I. Exponentially accelerated approach to stationarity in markovian open quantum systems through the mpemba effect. *Phys. Rev. Lett.* **127**, 060401 (2021).
- Nava, A. & Fabrizio, M. Lindblad dissipative dynamics in the presence of phase coexistence. *Phys. Rev. B* **100**, 125102 (2019).
- Kochsiek, S., Carollo, F. & Lesanovsky, I. Accelerating the approach of dissipative quantum spin systems towards stationarity through global spin rotations. *Phys. Rev. A* **106**, 012207 (2022).
- Manikandan, S. K. Equidistant quenches in few-level quantum systems. *Phys. Rev. Res.* **3**, 043108 (2021).
- Ares, F., Murciano, S. & Calabrese, P. Entanglement asymmetry as a probe of symmetry breaking. *Nat. Commun.* **14**, 2036 (2023).
- Rylands, C. et al. Microscopic origin of the quantum mpemba effect in integrable systems. *Phys. Rev. Lett.* **133**, 010401 (2024).
- Ivander, F., Anto-Sztrikacs, N. & Segal, D. Hyperacceleration of quantum thermalization dynamics by bypassing long-lived coherences: An analytical treatment. *Phys. Rev. E* **108**, 014130 (2023).
- Chatterjee, A. K., Takada, S. & Hayakawa, H. Quantum mpemba effect in a quantum dot with reservoirs. *Phys. Rev. Lett.* **131**, 080402 (2023).
- Chatterjee, A. K., Takada, S. & Hayakawa, H. Multiple quantum mpemba effect: exceptional points and oscillations. *Phys. Rev. A* **110**, 022213 (2024).
- Moroder, M., Culhane, O., Zawadzki, K. & Goold, J. Thermodynamics of the quantum mpemba effect. *Phys. Rev. Lett.* **133**, 140404 (2024).
- Boubakour, M., Endo, S., Fogarty, T. & Busch, T. Dynamical invariant based shortcut to equilibration in open quantum systems. arXiv:2401.11659 (2024).
- Joshi, L. K. et al. Observing the quantum mpemba effect in quantum simulations. *Phys. Rev. Lett.* **133**, 010402 (2024).
- Aharony Shapira, S. et al. Inverse mpemba effect demonstrated on a single trapped ion qubit. *Phys. Rev. Lett.* **133**, 010403 (2024).
- Lasanta, A., Vega Reyes, F., Prados, A. & Santos, A. When the hotter cools more quickly: Mpemba effect in granular fluids. *Phys. Rev. Lett.* **119**, 148001 (2017).
- Bender, C. M., Brody, D. C., Jones, H. F. & Meister, B. K. Faster than hermitian quantum mechanics. *Phys. Rev. Lett.* **98**, 040403 (2007).

33. Chen, W., Özdemir, Ş. K., Zhao, G., Wiersig, J. & Yang, L. Exceptional points enhance sensing in an optical microcavity. *Nature* **548**, 192 (2017).
34. Hodaei, H. et al. Enhanced sensitivity at higher-order exceptional points. *Nature* **548**, 187 (2017).
35. Miri, M. A. & Alù, A. Exceptional points in optics and photonics. *Science* **363**, eaar7709 (2019).
36. Minganti, F., Miranowicz, A., Chhajlany, R. W. & Nori, F. Quantum exceptional points of non-hermitian hamiltonians and liouvillians: the effects of quantum jumps. *Phys. Rev. A* **100**, 062131 (2019).
37. Naghiloo, M., Abbasi, M., Joglekar, Y. N. & Murch, K. W. Quantum state tomography across the exceptional point in a single dissipative qubit. *Nat. Phys.* **15**, 1232–1236 (2019).
38. Chen, W., Abbasi, M., Joglekar, Y. N. & Murch, K. W. Quantum jumps in the non-hermitian dynamics of a superconducting qubit. *Phys. Rev. Lett.* **127**, 140504 (2021).
39. Chen, W. et al. Decoherence induced exceptional points in a dissipative superconducting qubit. *Phys. Rev. Lett.* **128**, 110402 (2022).
40. Ding, K., Ma, G., Xiao, M., Zhang, Z. Q. & Chan, C. T. Emergence, coalescence, and topological properties of multiple exceptional points and their experimental realization. *Phys. Rev. X* **6**, 021007 (2016).
41. Zhou, Y.-L. et al. Accelerating relaxation through liouvillian exceptional point. *Phys. Rev. Res.* **5**, 043036 (2023).
42. Purkayastha, A., Kulkarni, M. & Joglekar, Y. N. Emergent \mathcal{PT} symmetry in a double-quantum-dot circuit qed setup. *Phys. Rev. Res.* **2**, 043075 (2020).
43. Zhang, J. W. et al. Dynamical control of quantum heat engines using exceptional points. *Nat. Commun.* **13**, 6225 (2022).
44. Bu, J.-T. et al. Enhancement of quantum heat engine by encircling a liouvillian exceptional point. *Phys. Rev. Lett.* **130**, 110402 (2023).
45. Macieszczak, K., Guță, M., Lesanovsky, I. & Garrahan, J. P. Towards a theory of metastability in open quantum dynamics. *Phys. Rev. Lett.* **116**, 240404 (2016).
46. Minganti, F., Biella, A., Bartolo, N. & Ciuti, C. Spectral theory of Liouvillians for dissipative phase transitions. *Phys. Rev. A* **98**, 042118 (2018).
47. Žnidarič, M. Relaxation times of dissipative many-body quantum systems. *Phys. Rev. E* **92**, 042143 (2015).
48. Nielsen, M. A. & Chuang, I. L. Quantum computation and quantum information (10th anniversary edition) (Oxford University Press, 2011).
49. Van Vu, T. & Hasegawa, Y. Geometrical bounds of the irreversibility in markovian systems. *Phys. Rev. Lett.* **126**, 010601 (2021).
50. García-Pintos, L. P., Nicholson, S. B., Green, J. R., del Campo, A. & Gorshkov, A. V. Unifying quantum and classical speed limits on observables. *Phys. Rev. X* **12**, 011038 (2022).
51. Orgad, D., Oganessian, V. & Gopalakrishnan, S. Dynamical transitions from slow to fast relaxation in random open quantum systems. *Phys. Rev. Lett.* **132**, 040403 (2024).
52. Ringbauer, M. et al. A universal qudit quantum processor with trapped ions. *Nat. Phys.* **18**, 1053–1057 (2022).
53. McKay, D. C., Wood, C. J., Sheldon, S., Chow, J. M. & Gambetta, J. M. Efficient Z gates for quantum computing. *Phys. Rev. A* **96**, 022330 (2017).
54. Thew, R. T., Nemoto, K., White, A. G. & Munro, W. J. Qudit quantum-state tomography. *Phys. Rev. A* **66**, 012303 (2002).
55. Hu, X.-M. et al. Self-testing of a single quantum system from theory to experiment. *npj Quantum Inf.* **9**, 103 (2023).
- Nos. 2023JJ30626 (Y.L.Z.), 2022RC1194 (J.Z.), 2023JJ10052 (J.Z.), National Natural Science Foundation of China under grant Nos. 12004430 (J.Z.), 12174448 (C.W.W.), 12074433 (P.X.C.), 12174447 (W.W.) and 12204543 (T.C.). H.J. is supported by the NSFC (grant No.11935006), the Science and Technology Innovation Program of Hunan Province (grant No. 2020RC4047), National Key R&D Program of China (No. 2024YFE0102400) and Hunan provincial major sci-tech program (No. 2023ZJ1010), and P.X.C. acknowledges the support from Innovation Program for Quantum Science and Technology under grant No. 2021ZD0301605.

Author contributions

Y.L.Z. conceived and designed the research with helpful discussions with H.J., W.L. and P.X.C.; J.Z. and G.X. were responsible for the experimental implementation, the data acquisition and its evaluation; J.Z., Y.L.Z. and C.W.W. designed the experiment with the help of T.C., Y.X., W.W. and P.X.C.; Y.L.Z. performed the simulations; Y.L.Z., J.Z. and G.X. analyzed the data; Y.L.Z., J.Z., H.J., W.L. and C.W.W. wrote the paper with inputs from G.X., T.C., Q.Z. and W.B.S.; H.J., W.L. and P.X.C. supervised this project. All authors discussed the results and contributed to the manuscript.

Competing interests

The authors declare no competing interests.

Additional information

Supplementary information The online version contains supplementary material available at <https://doi.org/10.1038/s41467-024-54303-0>.

Correspondence and requests for materials should be addressed to Weibin Li, Hui Jing or Yan-Li Zhou.

Peer review information *Nature Communications* thanks Antonio Lasanta, Pengfei Wang and the other, anonymous, reviewer(s) for their contribution to the peer review of this work. A peer review file is available.

Reprints and permissions information is available at <http://www.nature.com/reprints>

Publisher's note Springer Nature remains neutral with regard to jurisdictional claims in published maps and institutional affiliations.

Open Access This article is licensed under a Creative Commons Attribution-NonCommercial-NoDerivatives 4.0 International License, which permits any non-commercial use, sharing, distribution and reproduction in any medium or format, as long as you give appropriate credit to the original author(s) and the source, provide a link to the Creative Commons licence, and indicate if you modified the licensed material. You do not have permission under this licence to share adapted material derived from this article or parts of it. The images or other third party material in this article are included in the article's Creative Commons licence, unless indicated otherwise in a credit line to the material. If material is not included in the article's Creative Commons licence and your intended use is not permitted by statutory regulation or exceeds the permitted use, you will need to obtain permission directly from the copyright holder. To view a copy of this licence, visit <http://creativecommons.org/licenses/by-nc-nd/4.0/>.

© The Author(s) 2025

Acknowledgements

This work was supported by the Cornerstone foundation of NUDT (Y.L.Z.), Natural Science Foundation of Hunan Province of China under grant